

Optimization-Based Ramping Reserve Allocation of BESS for AGC Enhancement

Yiqiao Xu, *Student Member, IEEE*, Alessandra Parisio, *Senior Member, IEEE*, Zhongguo Li, *Member, IEEE*, Zhen Dong, *Member, IEEE*, and Zhengtao Ding, *Senior Member, IEEE*

Abstract—This paper presents a novel scheme termed Optimization-based Ramping Reserve Allocation (ORRA) for addressing an ongoing challenge in Automatic Generation Control (AGC) enhancement, i.e., the optimal coordination of multiple Battery Energy Storage Systems (BESSs). While exploiting further the synergy between BESSs and slow ramping resources, the proposed scheme offers an insight into the energy-neutral operation, which is achieved by smoothly discontinuing the BESS participation along with the minimization of Area Injection Error (AIE), a variant of traditional Area Control Error (ACE). The first stage of ORRA is to incorporate Neural Networks (NNs) with the AIE in order to ensure a zero-mean of ramping reserves to be allocated among BESSs. These AIE signals are then used to formulate the optimal coordination of BESS as an online optimization problem, which is therefore feedback-driven. Finally, a distributed optimization algorithm is developed to solve the formulated problem in real-time, achieving a sublinear dynamic regret that quantifies the cost difference to the trajectory computed by a centralized optimizer with perfect global information. Consistent with the geographical distribution of BESSs, the proposed ORRA is fully distributed such that the algorithm can be executed in parallel at all nodes. Simulations on a modified IEEE 14-bus system are performed to illustrate the effectiveness and important features of ORRA.

Index Terms—Battery Energy Storage System, Automatic Generation Control, Distributed Optimization.

I. INTRODUCTION

THE ambitious aim of replacing coal-based generation with Renewable Energy Sources (RESs) has aggravated the burden on frequency regulation due to immature management of RES [1], [2]. Recognizing the operational challenges faced by existing power systems, policymakers and Independent System Operators (ISOs) around the world have actively engaged in the commercial use of Battery Energy Storage Systems (BESSs) in the provision of grid services. Automatic Generation Control (AGC) is a balancing mechanism at the secondary control layer to cover the net-load forecasting errors in tens of seconds, which has the ultimate goal of minimizing Area Control Error (ACE) [3]. As various studies [4]–[6] have demonstrated, a reasonably sized BESS is able to improve AGC performance and mitigate the pressure on Conventional Generators (CGs) in recognition of two facts. First, the CG cannot switch directions instantly in response to a new dispatch target. Second, the BESS can provide symmetric support and be re-dispatched faster in both directions.

Over the decades, many utility-scale BESS projects with AGC functions have been commissioned, and there is a trend of coordinating multiple BESSs via a communication network to give substantial support. For example, Southern California Edison installed a 10 MW BESS and another 8 MW BESS at different transmission substations [4]. In Germany, an aggregated capacity of 90 MW/30 min BESS was equally distributed at six sites [7]. However, it has been observed that BESSs are not always able to efficiently minimize the ACE but sometimes give rise to counterproductive regulation [8]. This is partly due to the lack of explicit instructions on how much each BESS should contribute to AGC, whereas uncoordinated decision made by service providers is naturally self-interest [8]. Therefore, achieving the full potential of BESSs to benefit AGC is still an open challenge.

Different from traditional AGC systems that simply adopt a proportional-based allocation [9], a variety of optimization-based strategies have been proposed in recent research, based on Model Predictive Control (MPC) [10], [11], Approximate Dynamic Programming (ADP) [12], and Deep Reinforcement Learning (DRL) [13], [14]. DRL needs to be pre-trained with massive data and then deployed online (quite often, DRL has low sampling efficiency and poor adaptiveness to changing environments, e.g., weather). ADP and MPC can be directly implemented online but may require extensive computational power, especially when their prediction horizon is large. In contrast, online optimization is promising for real-time implementation since it requires notably less computational time for each iteration [15]. In [16], an online optimization policy is tailored for BESS to optimally follow the regulation signals, which, however, implements control until the optimum is reached. In [17], online optimization is combined with consensus algorithms to coordinate multiple BESSs in frequency regulation, but energy neutrality is not jointly considered.

Energy neutrality is a widely perceived concept requesting the cumulative energy input of a BESS to equal the output from a long-term view. Despite its significant importance to the operating integrity of BESS, it has not been taken seriously in many research studies [10]–[12], [14], [17]. As a consequence, some BESSs may have to move in opposition to what we expect for regulation to recover State-of-Charge (SoC) [18], or need to include a comprehensive SoC control such that the BESS acts only during designated periods [4]. For the sake of energy-neutral operation, PJM, an ISO in the US, transformed the ACE into a RegA signal for CGs and a RegD signal for fast ramping resources such as BESS.

The authors are with the Department of Electrical and Electronic Engineering, University of Manchester, Manchester M13 9PL, U.K. (e-mail: yiqiao.xu@manchester.ac.uk; zhengtao.ding@manchester.ac.uk).

The “hard-neutrality” imposed on the RegD signal kept the BESS from being over-charged or over-discharged but may force a considerable amount of RegD resources to act in the opposite direction of RegA resources [19]. Since 2017, PJM has switched to the conditional neutrality controller, a hybrid PID controller with an internal feedback loop that allows the RegD signal to be not strictly neutral but with a slight bias [20]. Midcontinent ISO (MISO) introduced a different scheme known as AGC enhancement, which places a priority on BESS in the provision of AGC and, more importantly, un-deploys them once the system frequency restores to the nominal value [21]. Compared to deliberately designing energy-neutral signals, this option directly utilizes the ACE to make better use of the ramping capabilities of BESSs. However, there are some practical issues associated with the use of AGC enhancement advocated by MISO. Most importantly, only when the frequency bias factor B accurately captures the Area’s Frequency Response Characteristic β , the numerical value of the ACE will be physically meaningful and zero-mean under Gaussian distributed net-load forecasting errors. Otherwise, miscalculated ACE can hedge against the efficient and energy-neutral operation of BESSs, and even a static bias uncertainty at 5% can have non-negligible impacts on settling time and cause unintended interaction between control areas [22].

The discrepancy between B and β , which we term bias uncertainty in this paper, is not uncommon owing to a contradiction arising in many markets that B is considered as a constant [23] while β tends to be highly dynamic and frequency-coupled. For instance, CGs will not adhere to the governor droop R^{-1} as specified with turbine-governor nonlinearity. Also, the load damping coefficient D can vary substantially with frequency conditions when there are a large number of frequency-responsive resources (FRRs) [24], aggregately modeled as a sectional droop in [25]. In [26], a Neural Network (NN)-based black-box model is proposed to reproduce the aggregated behavior of FRRs like BESS, but it has to be trained offline and will be unnecessarily complicated for the use of frequency regulation only. Meanwhile, the concept of Area Injection Error (AIE) has been proposed in [27], which corrects the ACE by removing the bias uncertainty manifested as turbine-governor nonlinearity, yet bias uncertainty caused by FRRs remains unresolved.

Compared to the previous work, the main contributions and highlights of this paper are summarized as follows:

- To ensure a zero-mean of ramping reserves provided by BESSs in the presence of turbine-governor nonlinearity and frequency-coupled load damping, we incorporate a NN-based black-box model [28] into the AIE signal design to account for bias uncertainty from both the load side and the generation side. Specifically, Radial Basis Function NNs (RBFNNs) are online interpolated to emulate the aggregated behavior of downstream FRRs.
- A novel scheme termed ORRA is designed to dynamically and optimally coordinate the responses of multiple BESSs in AGC. The proposed scheme is feedback-driven; along with the minimization of AIE, it can smoothly un-deploy BESSs by converging their powers back to zero. In

the long run, the accumulated battery exploitation will be negligible, virtually achieving energy-neutral operation.

- A distributed online optimization algorithm is developed for ORRA, where a dual-bounded technique [29] is integrated to relax the convergence requirements, and adaptive learning rates are designed to accelerate the optimization. The dynamic regret is used as a performance metric for the distributed algorithm versus its centralized counterpart with perfect global information. We prove that, under mild conditions, the algorithm provides a sublinear regret guarantee.
- Consistent with the geographical distribution of BESSs, the proposed ORRA is fully distributed such that algorithms can be executed in parallel at all nodes. Simulation studies demonstrate that ORRA can provide near-optimal and fair allocation of BESSs in real-time while significantly enhancing AGC performance.

The rest of this paper is structured as follows. AGC fundamentals, BESS models, and other preliminaries are introduced in Section II. Section III presents the novel scheme termed ORRA, the optimization algorithm, and key theoretical results. Comprehensive case studies in Section IV verify the effectiveness of ORRA through simulations on a modified IEEE 14-bus system. Section V concludes this paper.

II. PROBLEM FORMULATION

A. AGC Framework Considering Bias Uncertainty

An interconnected power system is usually partitioned into several control areas. An area has either an import or export of power and is tightly coupled with adjacent areas via tie-lines. After a disturbance occurs, CGs and BESSs are obliged to compensate for the net-load forecasting errors. The ACE is frequently used as a proxy error signal for instantaneous power imbalance, and it is obtained as the difference between scheduled and actual tie-line power flows ΔP^{tie} plus a scaled frequency deviation Δf , that is

$$ACE = \Delta P^{\text{tie}} + B\Delta f, \quad (1)$$

where B represents the frequency bias factor. As the numerical value of the ACE will be physically meaningful and zero-mean only when $B \approx D + R^{-1}$, the frequency bias should be set as close as possible to the AFRC, which is a combination of the load damping coefficient D and the governor droop R^{-1} .

It should be pointed out that such a linear governor droop response takes place only under ideal assumptions. Under the presence of governor-turbine nonlinearity, such as saturation and ramp-rate limits, CG’s mechanical power deviation in response to a frequency deviation is in fact a nonlinear function. For the CG at bus i , its mechanical power deviation ΔP_i^{m} can be described by

$$\Delta P_i^{\text{m}} = \Delta u_i^{\text{gov}} - \mathcal{F}_i(\Delta u_i^{\text{gov}}, \Delta f), \quad (2)$$

where $\mathcal{F}_i : \mathbb{R}^2 \rightarrow \mathbb{R}$ and Δu_i^{gov} is the governor input deviation. It indicates that obtaining an explicit analytical solution for B is difficult.

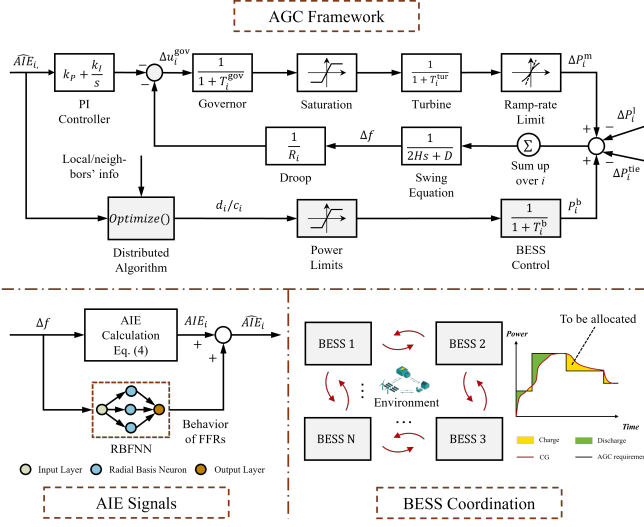


Fig. 1. A schematic overview of the proposed scheme including the AGC framework, the generation of AIE signals, and the coordination of BESSs.

Integrating (1) and (2) gives the concept of AIE [27], which is able to account for the governor-turbine nonlinearity using feedback of ΔP_i^{m}

$$AIE = \Delta P_i^{\text{tie}} + D' \Delta f + \sum_{i \in \mathcal{G}} (\Delta u_i^{\text{gov}} - \Delta P_i^{\text{m}}), \quad (3)$$

where D' is a tuning parameter associated with D and \mathcal{G} denotes the set of generator buses. Similarly, we denote \mathcal{V} as the set of buses, and then the AIE assigned to bus i will be

$$AIE_i = \sigma_i (\Delta P_i^{\text{tie}} + D' \Delta f) + \Delta u_i^{\text{gov}} - \Delta P_i^{\text{m}}, \quad (4)$$

for $i \in \mathcal{G}$ and $AIE_i = 0$ for $i \in \mathcal{V} - \mathcal{G}$, where $\sum_{i \in \mathcal{G}} \sigma_i = 1$. As reported in [27], the resultant AGC performance is subject to the tuning of D' . However, subsequent to increasing involvement of FRRs, their presence will bring additional load damping to existing power systems [30] and result in bias uncertainty on the load side. A difficulty to model the additional load damping D_A lies in that the value estimated based on the steady-state characteristics might be valid only for the operating condition where it has been derived. Thus, merely a static D' will not be able to reflect D_A that is frequency-coupled.

For the sake of an unbiased provision of ramping reserves that is critical to the energy-neutral operation, it is necessary to take into account also the aggregated behavior of downstream FRRs, denoted by ΔP_i^{fr} , when generating the AIE signals. Since that real-time monitoring of ΔP_i^{fr} incurs extra expenses and cannot be generalized, we propose to produce its approximation using online interpolated RBFNNs [28]. The goal is not to precisely model but emulate how these FRRs behave in response to different levels of frequency deviation based on a limited number of evaluations of $\Delta P_i^{\text{fr}}(\Delta f)$, which can be viewed as a massive accumulation of sectional droop functions [25].

Thus, the following improvements are made to the AIE signals defined by (4) so as to simultaneously address bias uncertainty from both the generation side and the load side:

$$\widehat{AIE}_i = AIE_i + \sum_{m=1}^M \omega_{i,m} \phi_i(\|\Delta f - \Delta f_m\|), \quad (5)$$

where the second term is the RBFNN interpolant of ΔP_i^{fr} , $\omega_{i,m}$ is a weighting factor that needs to be determined, M is the number of samples, and $\phi_i(x)$ is the widely applied Gaussian basis function

$$\phi_i(x) = \exp(-\xi x^2), \quad \xi \in \mathbb{R}_{>0}. \quad (6)$$

At the start of a new iteration, each node identifies whether next evaluation of $\Delta P_i^{\text{fr}}(\Delta f)$ should be conducted. If so, the regulation reserve provided by downstream FRRs connected at bus i will be collected along with the area frequency measurement. The set of these measurements with M samples is denoted by $\mathcal{M}_i = \{[\Delta f_{i,m}, \Delta P_{i,m}^{\text{fr}}(\Delta f)]^\top, \forall m \in \{1, \dots, M\}\}$. Note that a distance-based infill method is adopted from our previous work [28] to determine evaluation points for model improvement. The idea is to assure that the next evaluation point is held at a sufficient distance from the previously evaluated points ($\Delta f_{i,m}, \forall m \in \{1, \dots, M\}$).

Then, the interpolation matrix, also referred as Gram matrix, is updated according to

$$[G_i]_{rc} = \phi_i(\|\Delta f_{i,r} - \Delta f_{i,c}\|), \quad \forall r, c = 1, \dots, M, \quad (7)$$

and the weighting matrix, denoted by $\omega_i = [\omega_{i,1}, \dots, \omega_{i,M}]^\top$, is determined according to

$$\omega_i = (G_i^\top)^{-1} S_i, \quad (8)$$

where $S_i = [\Delta P_{i,1}^{\text{fr}}, \dots, \Delta P_{i,M}^{\text{fr}}]^\top$. There always exists a unique ω_i such that the RBFNN interpolant can reproduce observed behaviors [31]. By doing so, one may assume D' in (4) to be fixed at 1%-2.5% of the load [27]. A schematic overview of the proposed scheme is provided in Fig. 1.

B. BESS Model

Consider a battery operation defined over discrete time, where each control interval has a duration of τ . For the BESS deployed at bus i , its SoC at the next time instant $k+1$ can be described using a linear difference equation:

$$x_{i,k+1} = x_{i,k} + \frac{\eta^c \tau}{E_i} c_{i,k+1} - \frac{\tau}{\eta^d E_i} d_{i,k+1}, \quad (9)$$

where $x_{i,k+1}$ and $x_{i,k}$ are the SoC levels of BESS _{i} at time instant k and $k+1$, respectively; η^c and η^d are the charging/discharging efficiencies; E_i is the rated capacity; $c_{i,k+1}$ and $d_{i,k+1}$ denote the reference signals for charging and discharging and are treated as equivalent to the instantaneous BESS powers in this formulation, provided that the internal control loops are fast enough.

The BESS can either operate in charging or discharging mode. Irrespective of the model used, one has to avoid simultaneous charging and discharging. A convenient approach is

to invoke a binary variable $\delta_{i,k}$ that is determined according to

$$\delta_{i,k} = \frac{1}{2}(\widehat{AIE}_{i,k}/|\widehat{AIE}_{i,t}| + 1), \quad i \in \mathcal{G}, \quad (10a)$$

$$\delta_{i,k} = \delta_{j,k-\text{dist}(i,j)}, \quad i \in \mathcal{V} - \mathcal{G}, \quad (10b)$$

where $j \in \mathcal{G}$ exhibits the shortest path to i .

Note that the decision-making at time instant $k+1$ is based on the last observations at time instant k . Hence, we introduce the following constraints:

$$0 \leq c_{i,k+1} \leq (1 - \delta_{i,k}) \bar{c}_i, \quad (11)$$

$$0 \leq d_{i,k+1} \leq \delta_{i,k} \bar{d}_i, \quad (12)$$

such that the BESS is charged if $\delta_{i,k} = 0$ and discharged if $\delta_{i,k} = 1$, where \bar{c}_i and \bar{d}_i denote the BESS power limits.

To avoid over-charging and over-discharging, the SoC of each BESS needs to be restricted within an appropriate range:

$$\underline{x}_i \leq x_{i,k} + \frac{\eta^c \tau}{E_i} c_{i,k+1} - \frac{\tau}{\eta^d E_i} d_{i,k+1} \leq \bar{x}_i, \quad (13)$$

where \underline{x}_i and \bar{x}_i are the minimal and maximal SoC levels.

C. Cost Model

Cycling aging refers to a natural process leading to permanent battery degradation and is directly determined by the depth for which a battery is cycled. However, the resultant cost of cycling aging is usually omitted [6], [10], [32], [33] or approximated through a simplified model [17], [34], [35]. In contrast, we adopt a semi-empirical model that combines cycle identification results with experimental data [36].

Using the well-known rainflow-counting algorithm (due to space limits, please refer to [37]), we can identify the cycle depth of the latest half cycle per iteration

$$(\mu_{i,k}, \mathcal{R}_{i,k+1}) = \text{Rainflow}(x_{i,k}, \mathcal{R}_{i,k}), \quad (14)$$

where $\mu_{i,k}$ is the cycle depth between last two residues, $\mathcal{R}_{i,k+1}$ is the updated set of residues (the extrema unremoved by rainflow-counting algorithm), and $x_{i,k}$ is the latest SoC information, which together with $\mathcal{R}_{i,k}$ actually converts SoC trajectories that entail non-uniform fluctuations into consecutive cycles that can be full or half. A full cycle consists of a charge half cycle and a discharge half cycle, and it might be nested within other cycles once new SoC samples are acquired.

Subsequently, we are able to characterize the battery lifetime loss with respect to the identified half cycle as

$$\Delta L_{i,k}(\mu_{i,k}) := \frac{n_{i,k}^{\text{cyc}}}{2} a \mu_{i,k}^b, \quad (15)$$

where a and b are empirical coefficients [36] that normalize the cycling aging for a full cycle between 0 and 1, while $n_{i,k}^{\text{cyc}} \in (0, 1]$ calculates the number of cycles from the time indexes of the latest two residues. Additional quadratic terms on the BESS powers quantify the power wear. As a result, the battery usage cost (\$/h) is given as

$$f_{i,k}(d_{i,k}, c_{i,k}) := \underbrace{\theta_i^a \cdot (3600/\tau) \cdot \Delta L_{i,k}(\mu_{i,k})}_{\text{Cycling aging cost}} + \underbrace{\theta_i^b \cdot (d_{i,k} - c_{i,k})^2}_{\text{Power wear cost}}, \quad (16)$$

where θ_i^a and θ_i^b are cost coefficients taken from [16], [38]. by the chain rule, $f_{i,k}$ is convex with respect to $d_{i,k}$ and $c_{i,k}$ [16].

D. Optimization Problem Formulation

Consider N BESSs that are installed across a control area, where each BESS possesses a local cost function that cannot be revealed to the others. As illustrated in Fig. 2, the entire operation indexed by k can be divided into a number of optimization stages separated by the re-initialization of learning rates, which will be covered in III.A. We use t as an index for current optimization stage, with iteration 0 denoting its beginning and iteration $t+1$ denoting current position of optimization. For the ease of notation, $(\cdot)_{i,t}$ in current optimization stage is treated equivalent to $(\cdot)_{i,k}$ in the entire operation.

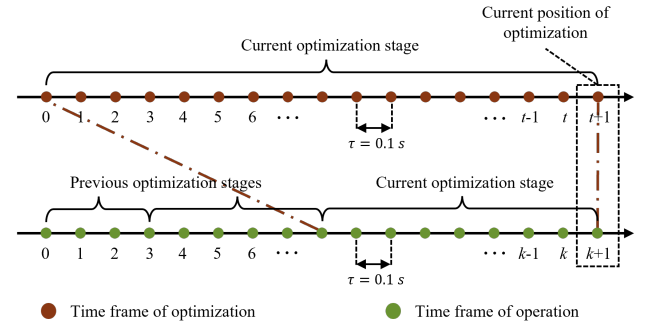


Fig. 2. Time frames of optimization indexed by t and battery operation indexed by k .

Here we would like to re-state that (17) is an online convex optimization problem with time-varying constraints, which requires BESS to first interact with the unknown environment and then observe the remaining AIE. In turn, each BESS will need to raise or lower its output at the next iteration $t+1$, based on the local and neighbors' observations at iteration t , to meet the instantaneous ramping requirements and thereby counteract the AIE. From this perspective, the optimization problem is feedback-driven, and in terms of cost minimization, it can be mathematically modeled as follows:

$$\min_{d_i, c_i} \sum_{i=1}^N f_{i,t}(d_i, c_i) \text{ subject to} \quad (17a)$$

$$\sum_{i=1}^N (d_i - c_i) = - \sum_{i=1}^N \widehat{AIE}_{i,t}, \quad (17b)$$

$$0 \leq c_i \leq (1 - \delta_{i,t}) \bar{c}_i, \quad (17c)$$

$$0 \leq d_i \leq \delta_{i,t} \bar{d}_i, \quad (17d)$$

$$\underline{x}_i \leq x_{i,t} + \frac{\eta^c \tau}{E_i} c_i - \frac{\tau}{\eta^d E_i} d_i \leq \bar{x}_i, \quad (17e)$$

where (17a) focuses on the real-time cost-effectiveness of AGC enhancement. Two decision variables, d_i and c_i , are optimized and then implemented at iteration $t+1$ (i.e., time instant $k+1$), where the binary variable $\delta_{i,t}$ is combined with (17b)–(17c) to decide whether charge or discharge at iteration

$t + 1$. Moreover, the calendar aging independent of charge-discharge cycling is omitted as it is a long-term process beyond the time frames of ORRA.

III. PROPOSED SCHEME

A. Distributed Online Optimization

First of all, the interconnected power system is modeled as a multi-agent system. Each BESS is managed by an agent that is responsible for information acquisition/exchange, computation, and algorithm execution and is partially aware of the global cost function and the global constraint due to grid infrastructure and privacy requirements. For the sake of generality, we denote

$$u_i := [d_i, -c_i]^\top, \quad h_{i,t}(u_i) := \mathbf{1}_2^\top u_i + \widehat{AIE}_{i,t}, \quad (18)$$

where $\mathbf{1}_2 = (1, 1) \in \mathbb{R}^2$.

Replace (17c)-(17e) with projection operation which projects u into its decision domain to meet the inequality constraints. Then the Lagrangian function associated with (17) can be reduced to

$$L_t(u, \lambda) = \sum_{i=1}^N f_{i,t}(u_i) + \lambda \sum_{i=1}^N h_{i,t}(u_i), \quad (19)$$

where λ is the dual variable of this problem.

A generalized algorithm to solve (19) is the Arrow-Hurwicz-Uzawa algorithm that searches for the saddle point of convex function using gradients of primal and dual variables of the Lagrangian function L_t . However, it seems evident from the following formula that the gradients involve global information such as λ and $\sum_{i=1}^N h_{i,t}(u_i)$

$$\frac{\partial L_t}{\partial u_i} = \left(\frac{\partial f_{i,t}}{\partial d_i}, -\frac{\partial f_{i,t}}{\partial c_i} \right) + \mathbf{1}_2 \lambda, \quad (20)$$

$$\frac{\partial L_t}{\partial \lambda} = \sum_{i=1}^N h_{i,t}(u_i). \quad (21)$$

Consider a peer-to-peer network for agent communication, which can be described by an undirected graph $\mathcal{G} = (\mathcal{V}, \mathcal{E})$, where $\mathcal{V} = \{1, \dots, N\}$ is the set of agents and $\mathcal{E} \subseteq \mathcal{V} \times \mathcal{V}$ is the set of communication links. Two agents are said to be neighboring if there exists a communication link between them. We introduce a matrix $W = [w_{ij}]$ to model the communication topology by setting $w_{ij} \in \mathbb{R}_{>0}$ for $(i, j) \in \mathcal{E}$ and $w_{ij} = 0$ otherwise. Note that W needs to be doubly-stochastic, that is to say, $\sum_{i=1}^N w_{ij} = \sum_{j=1}^N w_{ji} = 1$.

Two auxiliary variables are introduced as the local estimates of the global information λ and $\sum_{i=1}^N h_{i,t}(u_i)$ for each agent

$$\tilde{\lambda}_{i,t} := \sum_{j=1}^N w_{ij} \lambda_{j,t}, \quad \tilde{y}_{i,t} := \sum_{j=1}^N w_{ij} y_{j,t}. \quad (22)$$

which compute the weighted averaging of local and neighbors' information.

Then, using the local estimate of λ , we can rewrite (20) as

$$s_{i,t} = \left(\frac{\partial f_{i,t}}{\partial d_i}, -\frac{\partial f_{i,t}}{\partial c_i} \right) + \mathbf{1}_2 \tilde{\lambda}_{i,t}. \quad (23)$$

Based on (18) and (22)-(23), we develop an optimization algorithm to solve the time-varying problem (17) in a distributed, online fashion. The proposed algorithm is summarized in Algorithm 1.

Algorithm 1: Proposed Algorithm for ORRA

Input: parameters $\alpha, \beta, \gamma, \kappa_0, \epsilon_0 \in \mathbb{R}_{>0}$

- 1 Initialization of variables: $u_{i,0} \in \Omega_{i,0}, \lambda_{i,0} = 0,$
 $y_{i,0} = \mathbf{1}_2^\top u_{i,0} + \widehat{AIE}_{i,0};$
- 2 let $t \leftarrow 0;$
- 3 **while** TRUE **do**
- 4 **if** $t = 0$ **then**
- 5 Initialize learning rates: $\kappa_0 \in \mathbb{R}_{>0}, \epsilon_0 \in \mathbb{R}_{>0};$
- 6 **else**
- 7 Update learning rates: $\kappa_t = \kappa_0 t^{-\alpha}, \epsilon_t = \epsilon_0 t^{-\beta};$
- 8 **end**
- 9 **for** $i = 1, \dots, N$ **do**
- 10 Obtain local estimates $\tilde{\lambda}_{i,t}$ and $\tilde{y}_{i,t}$ using (22);
- 11 Obtain gradient search $s_{i,t}$ using (23);
- 12 Update $u_{i,t+1}$ and $\lambda_{i,t+1}$ based on
- 13 $u_{i,t+1} = \mathcal{P}_{\Omega_{i,t}}(u_{i,t} - \kappa_t s_{i,t}); \quad (24)$
- 14 $\lambda_{i,t+1} = (1 - \epsilon_t) \tilde{\lambda}_{i,t} + \gamma \kappa_t \tilde{y}_{i,t}; \quad (25)$
- 15 Obtain equality constraints on ramping reserve
 $h_{i,t}(u_{i,t+1})$ and $h_{i,t-1}(u_{i,t})$ using (18);
- 16 Update $y_{i,t+1}$ based on
- 17 $y_{i,t+1} = \tilde{y}_{i,t} + h_{i,t}(u_{i,t+1}) - h_{i,t-1}(u_{i,t}); \quad (26)$
- 18 **end**
- 19 let $t \leftarrow t + 1;$
- 20 **if** $t = T$ or $|\Delta f| \geq 0.05$ **then**
- 21 reset $t \leftarrow 0;$
- 22 **end**
- 23 **end**

Remark 1. The optimization is a feedback-driven process that leverages the AIE signals for online decision-making. Adaptive learning rates α and β are adopted, which start with high learning rates and smoothly decay at certain ratios. If certain conditions are met, i.e., t reaches the maximum iteration T or Δf exceeds the threshold on frequency deviation (0.05 Hz in this paper), the adaptive learning rates will be re-initialized to speed up the gradient search and rapidly compensate the AIE. Their definition domains, together with the regret analysis, can be found in Section III.B. The initial learning rates κ_0 and ϵ_0 , as well as $\gamma \in \mathbb{R}_{>0}$ need to be selected for a satisfactory stepsize.

Remark 2. Using Algorithm 1, local information of all nodes, namely $\lambda_{i,t}$ and $y_{i,t}$, can be aggregated via the sparse communication network per iteration to steadily enhance ORRA's perception of global information. At steady-state, we have $\lambda_t \rightarrow \bar{\lambda}_t$ and $y_t \rightarrow \bar{y}_t$ (also, $\tilde{\lambda}_t \rightarrow \bar{\lambda}_t$ and $\tilde{y}_t \rightarrow \bar{y}_t$), where $\bar{\lambda}_t := \mathbf{1}_N \sum_{i=1}^N \lambda_{i,t}/N$ and $\bar{y}_t := \mathbf{1}_N \sum_{i=1}^N y_{i,t}/N$. Projection operation $\mathcal{P}_{\Omega_{i,t}}$ in (24) is included to project decision variable $u_{i,t+1}$ into its decision domain $\Omega_{i,t}$. A dual-bounded technique [29] is integrated in (25) to impede the growth of $\lambda_{i,t}$ and relax the convergence requirements through ϵ_t . As CGs slightly adjust their outputs to cover the net-load forecasting errors, the BESSs will gradually withdraw their contribution to AGC.

This will ultimately lead to $d_T = \mathbf{0}_N$ and $c_T = \mathbf{0}_N$ if there are no further disturbances, which is of particular importance to avoid SoC drifts (the reader is referred to Fig. 5(a) in IV.A for the appearance of energy-neutral operation).

B. Regret Analysis

Due to the time-varying nature of online optimization, dynamic regret is introduced to define its convergence. This performance metric is computed for each iteration and summed up to measure how much the battery actions deviate from the best trajectory from an offline view. The dynamic regret at an arbitrary $T > 1$ is defined as

$$Reg(T) = \sum_{t=1}^T \sum_{i=1}^N f_{i,t}(u_{i,t}) - \sum_{t=1}^T \sum_{i=1}^N f_{i,t}(u_{i,t}^*). \quad (27)$$

Lemma 1. For any learning rates $\kappa_t, \epsilon_t \in \mathbb{R}_{>0}$, the following inequality always holds at an arbitrary $T > 1$

$$\begin{aligned} Reg(T) &\leq \sum_{t=1}^T \frac{1}{2\kappa_t} (\|u_t - u_t^*\|^2 - \|u_{t+1} - u_t^*\|^2) \\ &\quad + \sum_{t=1}^T \frac{1}{2\gamma\epsilon_t} (\|\bar{\lambda}_t\|^2 - \|\bar{\lambda}_{t+1}\|^2) \\ &\quad + \sum_{t=1}^T \frac{\kappa_t}{2} \|s_t\|^2 + \sum_{t=1}^T \frac{1}{2\gamma\kappa_t} \|\gamma\kappa_t \tilde{y}_t - \epsilon_t \bar{\lambda}_t\|^2 \\ &\quad + \sum_{t=1}^T \|\bar{\lambda}_t\| \cdot \|\tilde{y}_t - \bar{y}_t\| + \sum_{t=1}^T 2\|u_t\| \cdot \|\bar{\lambda}_t - \bar{\lambda}_t\|. \end{aligned} \quad (28)$$

Proof. The proof of Lemma 1 is provided in Appendix.A. \square

Lemma 2. Let learning rate $\kappa_t \in \mathbb{R}_{>0}$ and $T > 1$. Denote $S(T) := \sum_{t=1}^T (\|u_t - u_t^*\|^2 - \|u_{t+1} - u_t^*\|^2) / (2\kappa_t)$. Denote the bound on decision variables as B_u , where $B_u = \max(\bar{d}_i, \bar{c}_i, \forall i \in 1, \dots, N)$. Then, the following statement is true if and only if κ_t decreases progressively with t

$$S(T) \leq 2NB_u^2/\kappa_T + 2NB_u V(T). \quad (29)$$

Proof. The proof of Lemma 2 is provided in Appendix.B. \square

All these suggest that the boundedness of $Reg(T)$ relies on a sequence of results and the selection of learning rates. Note that the instantaneous dynamic regret $\sum_{i=1}^N f_{i,t}(u_{i,t}) - \sum_{i=1}^N f_{i,t}(u_{i,t}^*)$ may not perfectly converge to the exact value of zero due to a slight violation of (17b). However, the algorithm provides near-optimal operation and meets the constraints in most circumstances. The following assumptions are required to facilitate the derivation of our main results.

Assumption 1. 1) The local cost functions $f_{i,t} : \mathbb{R}^2 \rightarrow \mathbb{R}$ are Lipschitz continuous and there exists a positive constant C_f such that $\|\partial f_{i,t}(x)\| \leq C_f$ for $\forall i \in 1, \dots, N$ and $\forall t \in 0, \dots, T-1$.
2) The time-varying disturbances that the interconnected power system is subject to is norm-bounded, which means $\|h_{i,t}\|$ is bounded for $\forall i \in 1, \dots, N$ and $\forall t \in 0, \dots, T-1$.

Remark 3. This remark gives some important results for deriving the regret analysis. Under Assumption 1.2, there exists a constant $B_y > 0$ such that $\|y_{i,t}\|$ and $\|\tilde{y}_{i,t}\|$ are both uniformly bounded by B_y [39]. When digging into the updating law (25), we have $\|\tilde{\lambda}_{i,t+1}\| = \|(1 - \epsilon_t)\tilde{\lambda}_{i,t} + \gamma\tilde{y}_{i,t}\| \leq (1 - \epsilon_t)\|\tilde{\lambda}_{i,t}\| + \gamma B_y$. According to (22) and $\sum_{j=1}^N w_{ij} = 1$, one might expect $\|\tilde{\lambda}_{i,t+1}\| = \|\sum_{j=1}^N w_{ij} \lambda_{j,t+1}\| \leq \max(\|\lambda_{i,t+1}\|, \forall i \in 1, \dots, N)$. It can be easily verified by mathematical induction that $\|\lambda_{i,t}\|, \|\tilde{\lambda}_{i,t}\|, \|\bar{\lambda}_{i,t}\| \leq \gamma B_y \kappa_t / \epsilon_t$. Further we have $\|s_{i,t}\| \leq \|\partial f_{i,t}(u_{i,t})\| + \|\mathbf{1}_2 \tilde{\lambda}_{i,t}\| \leq C_f + 2\gamma B_y \kappa_t / \epsilon_t$.

Theorem 1. Let $0 < \alpha \leq \beta < 1$ and $V(T) := \sum_{t=1}^T \|u_{t+1}^* - u_t^*\| / \kappa_t$. Under Assumption 1 and Algorithm 1, it holds that $Reg(T) \in \mathcal{O}_+(T^{1+2\beta-3\alpha}) + \mathcal{O}_+(V_T)$. Furthermore, for the case that $\lim_{T \rightarrow \infty} V(T)/T \rightarrow 0$, one can ensure a sublinear dynamic regret with respect to T , i.e., $\lim_{T \rightarrow \infty} Reg(T)/T \rightarrow 0$ if $2\beta - 3\alpha \leq 0$ and $2\beta - \alpha - 1 \leq 0$.

Proof. Below, we are in a position to ensure the boundedness of each term of (28) by first identifying their asymptotic growth rates against T . Lemma 1 together with Assumption 1 lead to $\lim_{T \rightarrow \infty} S(T)/T = 0$. Now, the second term of (28) can be obtained as

$$\begin{aligned} &\sum_{t=1}^T \frac{1}{2\gamma\kappa_t} (\|\bar{\lambda}_t\|^2 - \|\bar{\lambda}_{t+1}\|^2) \\ &\leq \frac{N}{2\gamma} \left[\sum_{t=2}^T \left(\frac{1}{\kappa_t} - \frac{1}{\kappa_{t-1}} \right) \|\bar{\lambda}_{i,t}\|^2 + \frac{1}{\kappa_1} \|\bar{\lambda}_{i,1}\|^2 \right] \\ &< \frac{N}{2} \left[\sum_{t=2}^T \left(\frac{1}{\kappa_t} - \frac{1}{\kappa_{t-1}} \right) + \frac{1}{\kappa_1} \right] \cdot \left(\frac{\gamma B_y \kappa_T}{\epsilon_T} \right)^2 \\ &= \frac{N\gamma^2 B_y^2 \kappa_T}{2\epsilon_T^2} \\ &\in \mathcal{O}_+(T^{2\beta-\alpha}). \end{aligned} \quad (30)$$

By substituting $C_f + 2\gamma B_y / \epsilon_t$ for $\|s_{i,t}\|$ according to Remark 3, the third term of (28) becomes

$$\begin{aligned} &\sum_{t=1}^T \frac{\kappa_t}{2} \|s_t\|^2 \leq \sum_{t=1}^T \frac{N}{2} \kappa_t (C_f + 2\gamma B_y \kappa_t / \epsilon_t)^2 \\ &= \sum_{t=1}^T \frac{N}{2} [C_f^2 t^{-\alpha} + 4\gamma C_f B_y t^{\beta-2\alpha} + 4\gamma^2 B_y^2 t^{2\beta-3\alpha}] \\ &< \frac{N\gamma C_f^2}{2} \int_1^T t^{1-\alpha} dt + 2N\gamma C_f B_y \int_1^T t^{1+\beta-2\alpha} dt \\ &\quad + 2N\gamma B_y^2 \int_1^T t^{1+2\beta-3\alpha} dt + \text{const.} \\ &\in \mathcal{O}_+(T^{1+2\beta-3\alpha}). \end{aligned} \quad (31)$$

Similarly, invoking Remark 3 transfers the fourth term of

(28) into

$$\begin{aligned}
& \sum_{t=1}^T \frac{1}{2\gamma\kappa_t} \|\gamma\kappa_t \tilde{y}_t - \epsilon_t \bar{\lambda}_t\|^2 \\
& \leq \sum_{t=1}^T \frac{1}{2\gamma\kappa_t} (\gamma^2 B_y^2 \|\kappa_t\|^2 + \|\epsilon_t \bar{\lambda}_t\|^2 + 2\gamma B_y \|\kappa_t \epsilon_t \bar{\lambda}_t\|) \quad (32) \\
& = 2\gamma B_y^2 \sum_{t=1}^T \kappa_t \\
& \in \mathcal{O}_+(T^{1-\alpha}).
\end{aligned}$$

Furthermore, let us apply the results of [29] that $\sum_{t=1}^T \|\tilde{y}_t - \bar{y}_t\| \in \mathcal{O}_+(T^{1+\beta-2\alpha})$ and $\sum_{t=1}^T \|\bar{\lambda}_t - \tilde{\lambda}_t\| \in \mathcal{O}_+(T^{1-\alpha})$. Hence omitting the less significant terms associated with T allows us to conclude that

$$\begin{aligned}
& \sum_{t=1}^T \|\bar{\lambda}_t\| \cdot \|\tilde{y}_t - \bar{y}_t\| + \sum_{t=1}^T 2\|u_t\| \cdot \|\bar{\lambda}_t - \tilde{\lambda}_t\| \\
& \leq \frac{NB_y}{\epsilon_T} \sum_{t=1}^T \|\tilde{y}_t - \bar{y}_t\| + 4NB_u \sum_{t=1}^T \|\bar{\lambda}_t - \tilde{\lambda}_t\| \quad (33) \\
& \in \frac{NB_y \kappa_T}{\epsilon_T} \cdot \mathcal{O}_+(T^{1+\beta-2\alpha}) + 4NB_u \cdot \mathcal{O}_+(T^{1-\alpha}) \\
& \in \mathcal{O}_+(T^{1+2\beta-3\alpha}).
\end{aligned}$$

In the end, summarizing (28)-(33) completes the proof. \square

IV. SIMULATION STUDY

A modified IEEE-14 bus system is constructed based on MATLAB/Simulink environment, where two control areas (separated by the dotted line) with six CGs are specified, as shown in Fig. 3. It is supposed that the generation of RES is subject to variability and uncertainty and is treated as load fluctuations. It is worth remarking that we single out area 1 as the research object and consider BESS participation. Five BESSs are installed at different locations in Area 1 and each of them is allocated an agent. According to Theorem 1, we select $\alpha = 1/2$ and $\beta = 3/4$, while a control interval of 0.1s is considered. The communication network is illustrated in Fig 4, which can be mathematically described using a 5x5 matrix that is explained in Section III.A. Note that each line represents a two-way communication link between networked agents and the topology is rather flexible but should contain at least a path between any two agents. For each BESS, the capacity is 2 MWh, the peak power is 1 MW, the efficiencies for charging and discharging are both 0.95, and the initial SoC is arbitrarily chosen from [0.2, 0.8].

A. Case Study 1

This case study is provided as a calibration to examine the effectiveness and features of ORRA with respect to a step change. A load increase of 5 MW is introduced to Area 1 at $t = 10s$, and the simulation results are given in Fig. 5–Fig. 6. As it can be observed from Fig. 5(a), all BESSs contribute differently to AGC, owing to their intrinsic heterogeneities, and gradually detach from AGC by resettling their powers to zero. In Fig. 5(b), their marginal costs are maintained almost

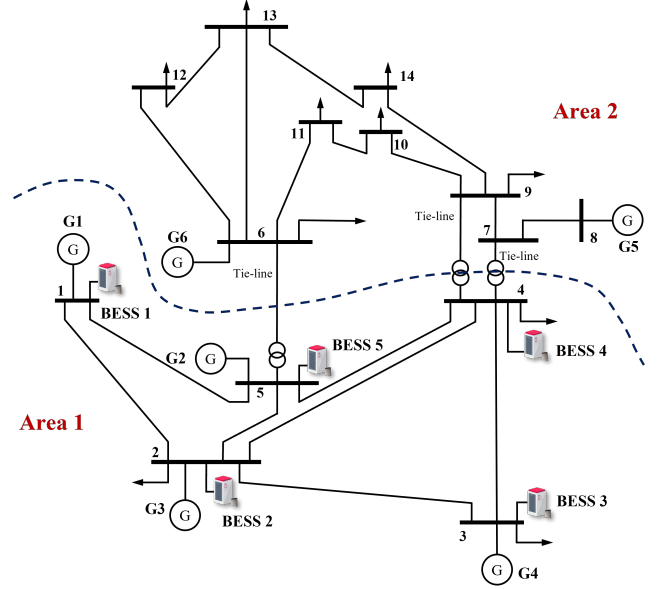


Fig. 3. Single-line diagram of the modified IEEE 14-bus system.

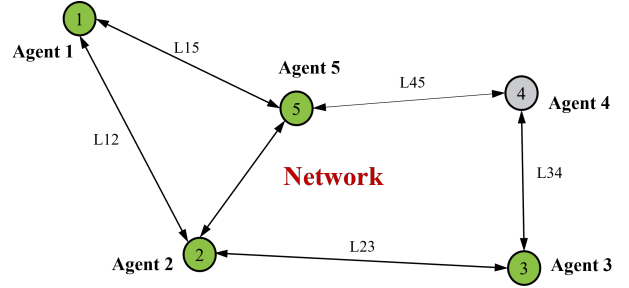


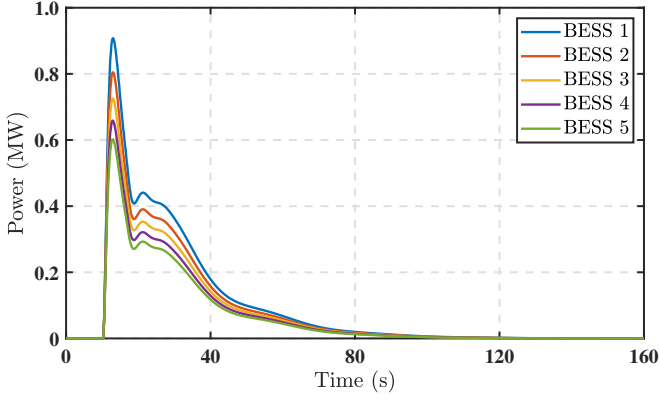
Fig. 4. Communication topology of five BESSs.

identical all the time, implying the fairness of allocation during the entire event.

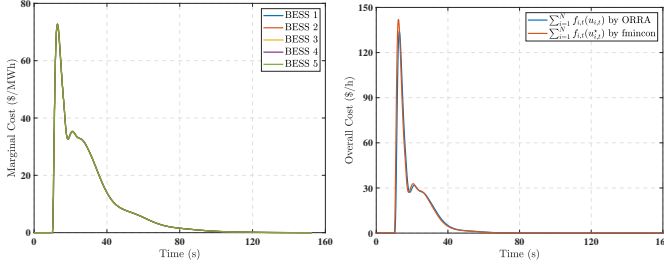
In Fig. 5(c), the instantaneous cost of all nodes of the proposed scheme is also compared with its centralized counterpart (MATLAB “fmincon” optimizer, a solver for constrained nonlinear convex optimization) having full access to global information, where the blue curve represents $\sum_{i=1}^N f_{i,t}(u_{i,t})$, the results of ORRA, and the red curve represents $\sum_{i=1}^N f_{i,t}(u_{i,t}^*)$, the results of “fmincon” from a centralized view. It can be seen that only slight inconsistency between $\sum_{i=1}^N f_{i,t}(u_{i,t})$ and $\sum_{i=1}^N f_{i,t}(u_{i,t}^*)$ is observed (mainly caused by the equality constraint not fully met) and our distributed scheme achieves the near-optimal allocation comparable to the centralized scheme, which is in line with the regret analysis in Section III.B.

Then, the proposed scheme are compared with three control groups and the results are given in Fig. 6. To avoid confusion, we outline that

- AIE+BESS: AIE-based AGC with BESS participation (i.e., the proposed scheme termed ORRA);
- ACE+BESS: ACE-based AGC with BESS participation;
- AIE: AIE-based AGC without BESS participation;
- ACE: ACE-based AGC without BESS participation.



(a) BESS powers converging to zero (the appearance of energy neutrality).



(b) BESS marginal costs.

(c) Overall battery usage cost.

Fig. 5. Optimization results regarding a 5 MW net-load change in Area 1.

Compared to the black lines marked with “ACE” and “AIE”, the magnitudes of frequency drops are greatly reduced in the presence of BESS participation due to the capabilities of responding fast and precisely they offered. It is worth noticing that the BESSs may fall into an inefficient regulation, as highlighted in Fig. 6 with red block, due to the miscalculation of ACE in the presence of bias uncertainty. As discussed in Section II.A, the ACE implicitly assumes a linear turbine-governor response and time-invariant load damping characteristic. On the contrary, the AIE permits a dynamic frequency bias to track with the AFRC and hence mitigates the impact of bias uncertainty. Consequently, the corresponding response displays a significant enhancement in AGC performance, which is quantified by comparing the responses of “AIE+BESS” and “AIE” and also highlighted in Fig. 6 with blue block.

B. Case Study 2

Seeing that ORRA was examined only under discharging mode, case study 2 is designed by extending the time span of case study 1 and introducing net-load fluctuations to further assess the effectiveness of ORRA. With positive values representing power deficiency and power surplus vice versus, the net-load fluctuations are generated as uniformly distributed random numbers ranging from -6 MW to 6 MW, as represented by the yellow dotted line in Fig 7(a). As a consequence, the BESSs have to frequently shift between discharging mode and charging mode to counteract the AIE. The blue line represents the total power of CGs and the red line represents the total power of BESSs. Instructed by the AIE signals, the

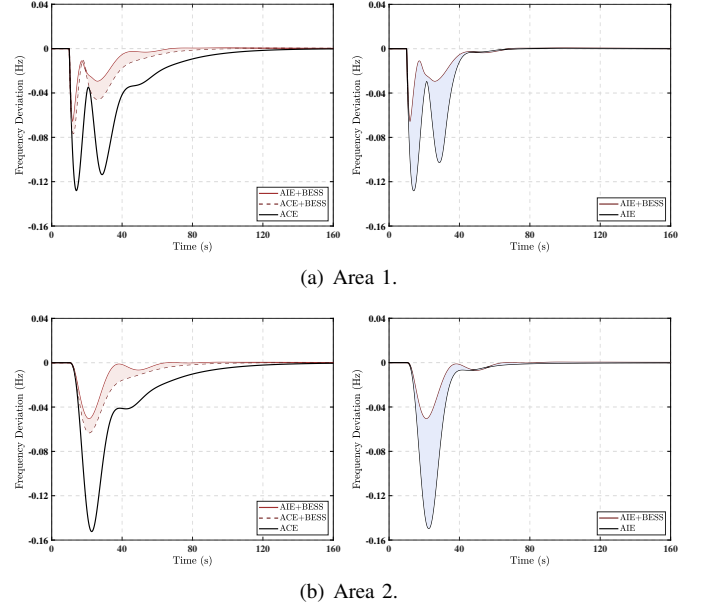
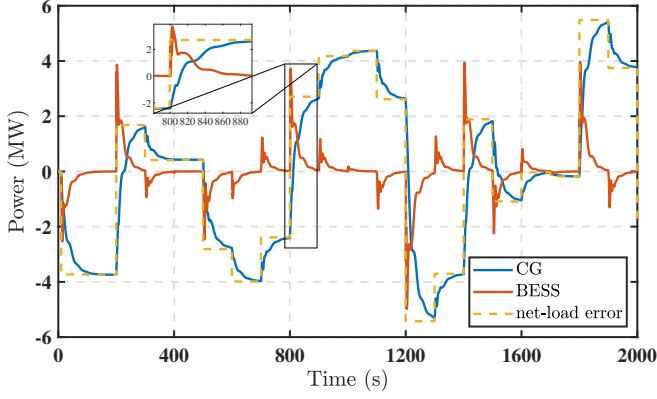


Fig. 6. Frequency Responses of two areas with respect to a 5 MW net-load change in Area 1. Inefficient regulation avoided by the use of AIE and AGC enhancement by BESS participation are respectively highlighted in red and blue.

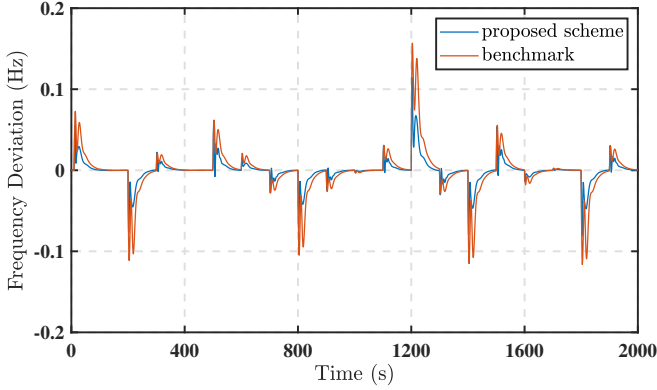
BESSs acts in collaboration with the CGs to correct the mismatch, showing a synergy between two classes of regulation resources. This synergy is particularly evident when CGs’ ramping capabilities are inadequate to meet the regulation requirements. For instance, in response to the disturbance at $t = 800s$, the CGs take about 100 seconds to ramp up to 2.7 MW and there clearly will be a gap in the provision of AGC without BESS participation. Furthermore, the frequency response under ORRA is compared with a benchmark system [10] to illustrate the advantages of ORRA, and the results are given in Fig. 7(b)–Fig. 7(c) illustrates the SoC levels over the entire time span. In the long run, the BESSs at a relatively low instantaneous power can significantly enhance AGC performance, and their operation is virtually energy-neutral as the SoC levels are closely kept around their initial values.

V. CONCLUSION

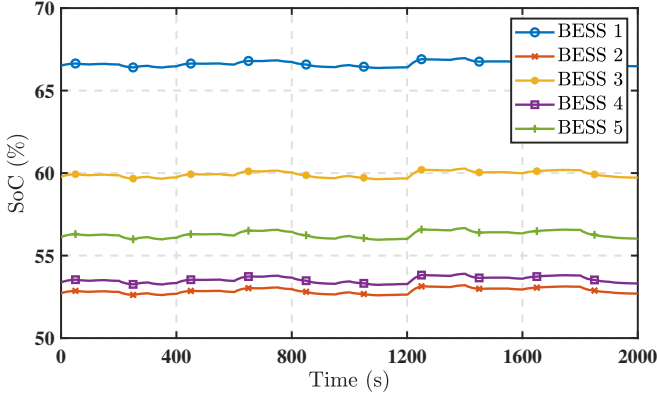
This paper is concerned with a novel scheme termed ORRA to dynamically and optimally coordinate multiple BESSs providing ramping capabilities to AGC. As the first step, we have employed NN-based black-box model to account for various bias uncertainty encountered during the operation of power systems, thereby ensuring a zero-mean of the AIE. A distributed online optimization algorithm has been developed for ORRA proven to be able to achieve a sublinear dynamic regret under mild conditions. A distinctive feature of ORRA is that the optimization is feedback-driven such that it can smoothly un-deploy BESSs by converging their powers back to zero along with the minimization of AIE, hence contributing to energy-neutral operation. Moreover, consistent with the geographical distribution of BESSs, the proposed ORRA is fully distributed.



(a) Total power of CGs, total power of BESSs, and net-load change (or forecasting error).



(b) Frequency responses of the proposed ORRA and a benchmark scheme based on robust MPC [10].



(c) Evolution of SoC levels over 30 minutes.

Fig. 7. Implementation of ORRA under net-load fluctuations.

VI. APPENDIX

A. Proof of Lemma 1

Proof. According to (19) and $\sum_{i=1}^N h_{i,t}(u_{i,t}^*) = 0$, we have that $Reg(T) \equiv \sum_{t=1}^T L_t(u_t, \mathbf{0}_N) - \sum_{t=1}^T L_t(u_t^*, \bar{\lambda}_t)$, which

allows us to rewrite the dynamic regret as

$$Reg(T) = \sum_{t=1}^T [L_t(u_t, \mathbf{0}_N) - L_t(u_t, \bar{\lambda}_t)] + \sum_{t=1}^T [L_t(u_t, \bar{\lambda}_t) - L_t(u_t^*, \bar{\lambda}_t)]. \quad (34)$$

To move forward, we need to obtain the upper bounds of $\sum_{t=1}^T [L_t(u_t, \mathbf{0}_N) - L_t(u_t, \bar{\lambda}_t)]$ and $\sum_{t=1}^T [L_t(u_t, \bar{\lambda}_t) - L_t(u_t^*, \bar{\lambda}_t)]$. From updating law (25), we have

$$\begin{aligned} \|\bar{\lambda}_{t+1}\|^2 &= \|\bar{\lambda}_t + (\gamma\kappa_t \tilde{y}_t - \epsilon_t \bar{\lambda}_t)\|^2 \\ &\leq \|\bar{\lambda}_t\|^2 + \|\gamma\kappa_t \tilde{y}_t - \epsilon_t \bar{\lambda}_t\|^2 + 2(\gamma\kappa_t \tilde{y}_t - \epsilon_t \bar{\lambda}_t)^\top \bar{\lambda}_t \\ &\leq \|\bar{\lambda}_t\|^2 + \|\gamma\kappa_t \tilde{y}_t - \epsilon_t \bar{\lambda}_t\|^2 + 2\gamma\kappa_t \tilde{y}_t^\top \bar{\lambda}_t. \end{aligned} \quad (35)$$

Since $\tilde{y}_t^\top \bar{\lambda}_t = (\tilde{y}_t - \bar{y}_t)^\top \bar{\lambda}_t + \bar{y}_t^\top \bar{\lambda}_t$ and $\bar{y}_t^\top \bar{\lambda}_t = L_t(u_t, \bar{\lambda}_t) - L_t(u_t, \mathbf{0}_N)$, (35) gives the result that the first term of (34) satisfies

$$\begin{aligned} &L_t(u_t, \mathbf{0}_N) - L_t(u_t, \bar{\lambda}_t) \\ &\leq \frac{1}{2\gamma\kappa_t} (\|\bar{\lambda}_t\|^2 - \|\bar{\lambda}_{t+1}\|^2) + \frac{1}{2\gamma\kappa_t} \|\gamma\kappa_t \tilde{y}_t - \epsilon_t \bar{\lambda}_t\|^2 \\ &\quad + \|\bar{\lambda}_t\| \cdot \|\tilde{y}_t - \bar{y}_t\|. \end{aligned} \quad (36)$$

As the next step, recalling updating law (24) along the property possessed by projection mapping that $\|\mathcal{P}_\Omega(x) - \mathcal{P}_\Omega(y)\| \leq \|x - y\|$ yields

$$\begin{aligned} \|u_{t+1} - u_t^*\|^2 &\leq \|u_t - u_t^* - \kappa_t s_t\|^2 \\ &\leq \|u_t - u_t^*\|^2 + \|\kappa_t s_t\|^2 \\ &\quad - 2\kappa_t s_t^\top (u_t - u_t^*). \end{aligned} \quad (37)$$

By the first-order property of characterization of convex functions, we have $-2\kappa_t s_t^\top (u_t - u_t^*) \leq -2\kappa_t [f_t(u_t) - f_t(u_t^*) + (\mathbf{1}_2 \bar{\lambda}_t)^\top (u_t - u_t^*)]$. As a result of $f_t(u_t) - f_t(u_t^*) = L_t(u_t, \bar{\lambda}_t) - L_t(u_t^*, \bar{\lambda}_t)$, we can further conclude that

$$\begin{aligned} &L_t(u_t, \bar{\lambda}_t) - L_t(u_t^*, \bar{\lambda}_t) \\ &\leq \frac{1}{2\kappa_t} (\|u_t - u_t^*\|^2 - \|u_{t+1} - u_t^*\|^2) + \frac{\kappa_t}{2} \|s_t\|^2 \\ &\quad + 2\|u_t\| \cdot \|\bar{\lambda}_t - \bar{\lambda}_t\|. \end{aligned} \quad (38)$$

Substituting (36) and (38) into (34) and rearranging the terms ends the proof. \square

B. Proof of Lemma 2

Proof. We regroup $S(T)$ as the summation of $S_1(T)$ and $S_2(T)$ for notational simplicity, as shown by

$$\begin{aligned} S(T) &= \underbrace{\sum_{t=1}^T \frac{1}{2\kappa_t} (\|u_t - u_t^*\|^2 - \|u_{t+1} - u_{t+1}^*\|^2)}_{S_1(T)} \\ &\quad + \underbrace{\sum_{t=1}^T \frac{1}{2\kappa_t} (\|u_{t+1} - u_{t+1}^*\|^2 - \|u_{t+1} - u_t^*\|^2)}_{S_2(T)}. \end{aligned} \quad (39)$$

By taking the similar approach alike (30), $S_1(T)$ can be rearranged as

$$\begin{aligned} S_1(T) &= \frac{1}{2\kappa_1} \|u_1 - u_1^*\| - \frac{1}{2\kappa_{T+1}} \|u_{T+1} - u_{T+1}^*\| \\ &\quad + \frac{1}{2} \sum_{t=2}^T \left(\frac{1}{\kappa_t} - \frac{1}{\kappa_{t-1}} \right) \|u_t - u_t^*\|^2 \\ &\leq 2NB_u^2/\kappa_T. \end{aligned} \quad (40)$$

From $\|x\|^2 - \|y\|^2 \leq \|x + y\| \cdot \|x - y\|$, it can be easily seen that

$$\begin{aligned} S_2(T) &\leq \sum_{t=1}^T \frac{1}{2\kappa_t} (2\|u_{t+1}\| + \|u_{t+1}^*\| + \|u_t^*\|) \cdot \|u_t^* - u_{t+1}^*\| \\ &\leq 2NB_u V(T). \end{aligned} \quad (41)$$

Combining the results of (40) and (41) completes the proof. \square

REFERENCES

- [1] G. P. Holdmann, R. W. Wies, and J. B. Vandermeer, "Renewable energy integration in Alaska's remote islanded microgrids: Economic drivers, technical strategies, technological niche development, and policy implications," *Proc. IEEE*, vol. 107, no. 9, pp. 1820–1837, 2019.
- [2] T. Anderson, M. Muralidharan, P. Srivastava, H. V. Haghi, J. Cortés, J. Kleissl, S. Martínez, and B. Washom, "Frequency regulation with heterogeneous energy resources: A realization using distributed control," *IEEE Trans. Smart Grid*, vol. 12, no. 5, pp. 4126–4136, 2021.
- [3] N. Jaleeli, L. S. VanSlyck, D. N. Ewart, L. H. Fink, and A. G. Hoffmann, "Understanding automatic generation control," *IEEE Trans. Power Syst.*, vol. 7, no. 3, pp. 1106–1122, 1992.
- [4] X. Xie, Y. Guo, B. Wang, Y. Dong, L. Mou, and F. Xue, "Improving AGC performance of coal-fueled thermal generators using multi-MW scale BESS: A practical application," *IEEE Trans. Smart Grid*, vol. 9, no. 3, pp. 1769–1777, 2018.
- [5] Y. Tan, K. M. Muttaqi, P. Ciufo, L. Meegahapola, X. Guo, B. Chen, and H. Chen, "Enhanced frequency regulation using multilevel energy storage in remote area power supply systems," *IEEE Trans. Power Syst.*, vol. 34, no. 1, pp. 163–170, 2019.
- [6] K. Doenges, I. Egido, E. L. M. L. Sigris, and L. Rouco, "Improving AGC performance in power systems with regulation response accuracy margins using battery energy storage system (BESS)," *IEEE Trans. Power Syst.*, vol. 35, no. 4, pp. 2816–2825, 2020.
- [7] STEAG GmbH, "Optimized operation of large-scale battery systems—Experience, new opportunities and big data." [Online]. Available: https://www.steag-energyservices.com/uploads/pics/Electrify_Europe_Optimized_operation_of_large_scale_battery_systems_protect_discretionary{\char\hyphenchar\font}{\}_experiences_new_opportunities_and_big_data_eng_13.pdf
- [8] PJM, "Fast response regulation (RegD) resources operational impact," 2015. [Online]. Available: [https://www.pjm.com/{\sim\\$}/media/committees-groups/committees/oc/20150701-rpi/20150701-fast-response-regulation-resources-operational-impact-problem-statement-ashx](https://www.pjm.com/{\sim$}/media/committees-groups/committees/oc/20150701-rpi/20150701-fast-response-regulation-resources-operational-impact-problem-statement-ashx)
- [9] Y. Cheng, M. Tabrizi, M. Sahni, A. Povedano, and D. Nichols, "Dynamic available AGC based approach for enhancing utility scale energy storage performance," *IEEE Trans. Smart Grid*, vol. 5, no. 2, pp. 1070–1078, 2014.
- [10] A. Oshnoei, M. Kheradmandi, and S. M. Muyeen, "Robust control scheme for distributed battery energy storage systems in load frequency control," *IEEE Trans. Power Syst.*, vol. 35, no. 6, pp. 4781–4791, 2020.
- [11] O. Stanojev, U. Markovic, P. Aristidou, G. Hug, D. S. Callaway, and E. Vrettos, "MPC-based fast frequency control of voltage source converters in low-inertia power systems," *IEEE Trans. Power Syst.*, 2020.
- [12] X. Xue, X. Ai, J. Fang, S. Cui, Y. Jiang, W. Yao, Z. Chen, and J. Wen, "Real-time schedule of microgrid for maximizing battery energy storage utilization," *IEEE Trans. Sustain. Energy*, pp. 1–1, 2022.
- [13] H. Shuai, F. Li, H. Pulgar-Painemal, and Y. Xue, "Branching dueling Q-network-based online scheduling of a microgrid with distributed energy storage systems," *IEEE Trans. Smart Grid*, vol. 12, no. 6, pp. 5479–5482, 2021.
- [14] B. Huang and J. Wang, "Deep-reinforcement-learning-based capacity scheduling for PV-battery storage system," *IEEE Trans. Smart Grid*, vol. 12, no. 3, pp. 2272–2283, 2021.
- [15] S. Shalev-Shwartz, "Online learning and online convex optimization," *Foundations and Trends® in Machine Learning*, vol. 4, no. 2, pp. 107–194, 2012.
- [16] Y. Shi, B. Xu, D. Kirschen, and B. Zhang, "Optimal battery control under cycle aging mechanisms in pay for performance settings," *IEEE Trans. Automat. Contr.*, vol. 64, no. 6, pp. 2324–2339, 2019.
- [17] T. Zhao, A. Parisio, and J. V. Milanović, "Distributed control of battery energy storage systems for improved frequency regulation," *IEEE Trans. Power Syst.*, vol. 35, no. 5, pp. 3729–3738, 2020.
- [18] P. H. Divshali and C. Evens, "Optimum operation of battery storage system in frequency containment reserves markets," *IEEE Trans. Smart Grid*, vol. 11, no. 6, pp. 4906–4915, 2020.
- [19] N. S. Guzman, M. Arriaga, C. A. Canizares, J. W. Simpson-Porco, D. Sohm, and K. Bhattacharya, "Regulation signal design and fast frequency control with energy storage systems," *IEEE Trans. Power Syst.*, 2021.
- [20] PJM, "Implementation and rationale for PJM's conditional neutrality regulation signals," 2017. [Online]. Available: [https://www.pjm.com/{\sim\\$}/media/committees-groups/task-forces/rmistf/postings/regulation-market-whitepaper.ashx](https://www.pjm.com/{\sim$}/media/committees-groups/task-forces/rmistf/postings/regulation-market-whitepaper.ashx)
- [21] W. Li and Y. Chen, "MISO AGC enhancement proposal to better utilize fast ramping resources," in *Proc. IEEE Power Energy Soc. Gen. Meet.*, 2015.
- [22] M. H. Syed, E. Guillo-Sansano, S. M. Blair, G. M. Burt, A. M. Prostejovsky, and E. Rikos, "Enhanced load frequency control: incorporating locational information for temporal enhancement," *IET Generation, Transmission & Distribution*, vol. 13, no. 10, pp. 1865–1874, 2019.
- [23] PJM, "PJM manual 12: Balancing operations," 2021. [Online]. Available: [https://www.pjm.com/{\sim\\$}/media/documents/manuals/m12.ashx](https://www.pjm.com/{\sim$}/media/documents/manuals/m12.ashx)
- [24] S. Liao, J. Xu, Y. Sun, W. Gao, X.-Y. Ma, M. Zhou, Y. Qu, X. Li, J. Gu, and J. Dong, "Load-damping characteristic control method in an isolated power system with industrial voltage-sensitive load," *IEEE Trans. Power Syst.*, vol. 31, no. 2, pp. 1118–1128, 2016.
- [25] X. Zhu, M. Xia, and H.-D. Chiang, "Coordinated sectional droop charging control for EV aggregator enhancing frequency," *Appl. Energy*, vol. 210, pp. 936–943, 2018.
- [26] F. Calero, C. A. Cañizares, and K. Bhattacharya, "Aggregated BESS dynamic models for active distribution network studies," *IEEE Trans. Smart Grid*, vol. 12, no. 3, pp. 2077–2088, 2021.
- [27] J. W. Simpson-Porco, "On area control errors, area injection errors, and textbook automatic generation control," *IEEE Trans. Power Syst.*, vol. 36, no. 1, pp. 557–560, 2021.
- [28] Z. Li, Z. Dong, Z. Liang, and Z. Ding, "Surrogate-based distributed optimisation for expensive black-box functions," *Automatica*, vol. 125, p. 109407, 2021.
- [29] X. Li, X. Yi, and L. Xie, "Distributed online optimization for multi-agent networks with coupled inequality constraints," *IEEE Trans. Automat. Contr.*, vol. 66, no. 8, pp. 3575–3591, 2021.
- [30] V. Gholamrezaie, M. G. Dozein, H. Monsef, and B. Wu, "An optimal frequency control method through a dynamic load frequency control (LFC) model incorporating wind farm," *IEEE Syst. J.*, vol. 12, no. 1, pp. 392–401, 2018.
- [31] W. Yao, X. Chen, Y. Huang, and M. van Tooren, "A surrogate-based optimization method with RBF neural network enhanced by linear interpolation and hybrid infill strategy," *Optim. Methods Software*, vol. 29, no. 2, pp. 406–429, 2014.
- [32] D. Zhu and Y. A. Zhang, "Optimal coordinated control of multiple battery energy storage systems for primary frequency regulation," *IEEE Trans. Power Syst.*, vol. 34, no. 1, pp. 555–565, 2019.
- [33] L. Xing, Y. Mishra, Y.-C. Tian, G. Ledwich, H. Su, C. Peng, and M. Fei, "Dual-consensus-based distributed frequency control for multiple energy storage systems," *IEEE Trans. Smart Grid*, vol. 10, no. 6, pp. 6396–6403, 2019.
- [34] L. Sun, J. Qiu, X. Han, X. Yin, and Z. Dong, "Per-use-share rental strategy of distributed BESS in joint energy and frequency control ancillary services markets," *Appl. Energy*, vol. 277, p. 115589, 2020.
- [35] N. Padmanabhan, M. Ahmed, and K. Bhattacharya, "Battery energy storage systems in energy and reserve markets," *IEEE Trans. Power Syst.*, vol. 35, no. 1, pp. 215–226, 2020.

- [36] I. Laresgoiti, S. Käbitz, M. Ecker, and D. U. Sauer, "Modeling mechanical degradation in lithium ion batteries during cycling: Solid electrolyte interphase fracture," *J. Power Sources*, vol. 300, pp. 112–122, 2015.
- [37] C. Amzallag, J. Gerey, J. Robert, and J. Bahuaud, "Standardization of the rainflow counting method for fatigue analysis," *Int. J. Fatigue*, vol. 16, no. 4, pp. 287–293, 1994.
- [38] Y. Liu, H. B. Gooi, and H. Xin, "Distributed energy management for the multi-microgrid system based on ADMM," in *Proc. IEEE Power Energy Soc. Gen. Meet.*, 2017, pp. 1–5.
- [39] S. Lee and M. M. Zavlanos, "On the sublinear regret of distributed primal-dual algorithms for online constrained optimization," *arXiv preprint arXiv:1705.11128*, 2017.